Petapascal Pressure Driven by Fast Isochoric Heating with a Multipicosecond Intense Laser Pulse

Kazuki Matsuo,[1] Naoki Higashi,[1] Natsumi Iwata,[1] Shohei Sakata,[1] Seungho Lee,[1] Tomoyuki Johzaki,[2] Hiroshi Sawada,[3] Yuki Iwasa,[1] King Fai Farley Law,[1] Hiroki Morita,[1] Yugo Ochiai,[1] Sadaoki Kojima,[1] Yuki Abe,[1] Masayasu Hata,[1] Takayoshi Sano,[1] Hideo Nagatomo,[1] Atsushi Sunahara,[4,5] Alessio Morace,[1] Akifumi Yogo,[1] Mitsuo Nakai,[1] Hitoshi Sakagami,[6] Tetsuo Ozaki,[6] Kohei Yamanoi,[1] Takayoshi Norimatsu,[1] Yoshiki Nakata,[1] Shigeki Tokita,[1] Junji Kawanaka,[1] Hiroyuki Shiraga,[1] Kunioki Mima,[1,7] Hiroshi Azechi,[1] Ryosuke Kodama,[1] Yasunobu Arikawa,[1] Yasuhiko Sentoku,[1] and Shinsuke Fujioka[1]

[1]*Institute of Laser Engineering, Osaka University, 2-6 Yamada-oka, Suita, Osaka 565-0871, Japan*
[2]*Hiroshima University, 1-4-1 Kagamiyama, Higashi-Hiroshima 739-8527, Japan*
[3]*Department of Physics, University of Nevada Reno, Reno, Nevada 89557, USA*
[4]*Institute for Laser Technology, 1-8-4 Utsubo-honmachi, Nishi-ku Osaka, Osaka, 550-0004, Japan*
[5]*Center of Materials Under eXtreame Environment, Purdue University, 500 Central Drive, West Lafayette, Indiana 47907, USA*
[6]*National Institute for Fusion Science, National Institutes of Natural Sciences, 322-6 Oroshi, Toki, Gifu, 509-5292, Japan*
[7]*The Graduate School for the Creation of New Photonics Industries, 1955-1 Kurematsu, Nishi-ku, Hamamatsu, Shizuoka 431-1202, Japan*

(Received 27 August 2019; revised manuscript received 12 November 2019; published 24 January 2020)

Fast isochoric laser heating is a scheme to heat matter with a relativistic intensity ($> 10^{18}$ W/cm^2) laser pulse for producing an ultrahigh-energy-density (UHED) state. We have demonstrated an efficient fast isochoric heating of a compressed dense plasma core with a multipicosecond kilojoule-class petawatt laser and an assistance of externally applied kilotesla magnetic fields for guiding fast electrons to the dense plasma. A UHED state of 2.2 PPa is achieved experimentally with 4.6 kJ of total laser energy that is one order of magnitude lower than the energy used in the conventional implosion scheme. A two-dimensional particle-in-cell simulation confirmed that diffusive heating from a laser-plasma interaction zone to the dense plasma plays an essential role to the efficient creation of the UHED state.

DOI: 10.1103/PhysRevLett.124.035001

A power laser apparatus can inject plenty of energy into matter in a small volume within a short time duration. The matter becomes a high-energy density state that is applicable to various areas of scientific research such as laboratory astrophysics [1] and several kinds of radiation sources: x rays, charged particles, and neutrons [2,3]. Fast isochoric heating of a solid target has been studied to create high-energy density states by using a short pulse laser [4] and x-ray free electron laser [5,6]. The fast isochoric laser heating of a compressed dense plasma core is one of the schemes to create an ultrahigh-energy-density (UHED) state, which is equivalent to the state at the center of the Sun, for inertial confinement fusion (ICF) science.

In conventional implosion, the kinetic energy of an imploded shell is converted to the internal energy of the compressed matter at the maximum compression timing. A UHED state with 36 PPa (petapascal) was achieved at the National Ignition Facility with 1.8 MJ of laser energy by the indirect x-ray driven implosion [7]. The OMEGA laser facility with 30 kJ of laser energy produced 5.6 PPa of UHED by direct laser-driven implosion [8]. The significant growth of hydrodynamic instabilities during compression causes the hot spark mixing with the cold dense fuel and prevents an efficient creation of the UHED state. The current central ignition scheme requires enormous laser energy to create a UHED state. In this Letter, we report the production of the UHED state of 2.2 PPa with 4.6 kJ of total laser energy by using the fast isochoric heating of a compressed dense plasma core.

In the context of ICF, the fast isochoric heating also known as fast ignition had been proposed as an alternative approach to the ICF ignition [9]. This approach separates compression and heating processes to avoid the mixing, using a more stable compression followed by an external energy injection, whose timescale is much shorter than the implosion timescale. Significant progress has been made on fast isochoric heating to increase laser-to-core energy coupling [10–12]. Those improvements mainly focus on increasing laser-to-core energy coupling by drag heating which is the energy exchange through binary collisions between relativistic electrons (REs) and bulk electrons of the plasma. A postshot numerical simulation reveals that the other heating process called diffusive heating is essential to produce 2.2 PPa in this work.

There are three major mechanisms of fast isochoric heating [13]. The first mechanism is heating by REs

[14], which is often called drag heating. The REs' large divergence is a critical issue in drag heating. Enhancement of the laser-to-matter energy coupling with the magnetized fast isochoric heating scheme was reported by Ref. [14]. The maximum coupling efficiency via drag heating reached $7.7\% \pm 1.2\%$ because of the reduction of RE's divergence by the application of the external magnetic field. The second mechanism is resistive heating. The RE current drives the return current to maintain current neutrality in a plasma. Since the return current is more collisional than the RE current, the return current heats the plasma Ohmically. The resistive heating is the dominant heating mechanism in the laser-plasma interaction region. The third mechanism is diffusive heating, in which thermal electrons transport their energy diffusively from the laser heated hot region to the cold dense region. The diffusive heating has been identified as one of the dominant mechanisms for laser isochoric heating for the first time in Ref. [4]. A high ionization state in a solid was produced by thermal diffusion in a few picoseconds even after the pulse terminates. By extending the pulse duration, the laser supplies its energy continuously to the hot plasma while the thermal diffusion takes place. The diffusive heating becomes more important to heat the dense core (> 10 g/cm^3) beyond keV by multi-picosecond heating laser pulse duration.

Table I summarizes the results in this experiment. The experiment had been conducted at the GEKKO-LFEX laser facility at the Institute of Laser Engineering, Osaka University. The laser conditions, the laser-to-core coupling efficiency by drag heating, the geometrical positions of the target, and the diagnostics were identical to those of our previous experiment [14,15]. The experimental time origin ($t_{\mathrm{exp}} = 0$ ns) is defined hereafter as the peak of the compression laser pulse.

Three of the GEKKO-XII laser beams were used for generating the magnetic field to guide REs and enhance drag heating efficiency. The wavelength, pulse shape, pulse duration, and energy of the GEKKO-XII beams used for magnetic field generation were 1.053 μm, Gaussian, 1.3 ns full-width at half-maximum (FWHM), and 600 ± 20 J per beam. The strength of the magnetic field generated with the capacitor-coil target had been measured on GEKKO-XII, LULI2000, Shengguang-II, and OMEGA-EP laser facilities [21–25]. 600–700 T of magnetic fields were obtained by the current GEKKO-XII laser beam configuration. By applying external magnetic fields to the path of the REs and the thermalized electrons, which carry the heat, the divergence issue can be resolved [26] so that resistive heating near the interaction zone works efficiently to make a large temperature gradient for diffusive heating.

Six of the GEKKO-XII laser beams were used for the compression of a solid ball target. The wavelength, pulse shape, pulse duration, and energy of the GEKKO-XII beams used for implosion were 0.526 μm, Gaussian, 1.3 ns (FWHM), and 240 ± 15 J per beam. The target was made of a 200 μm-diameter Cu(II) oleate solid ball [$\mathrm{Cu}(\mathrm{C_{17}H_{33}COO})_2$] [27] coated with a 25 μm-thick polyvinyl alcohol layer to prevent the Cu atoms from direct laser irradiation. The Cu(II) oleate solid ball contains 9.7% Cu atoms in weight. X-ray emissions from Cu atoms were used for characterizing the coupling efficiency and the electron temperature. An open-tip gold cone was attached to the Cu (II) oleate solid ball. The solid ball compression does not generate shocks and rarefactions traveling ahead of the shock-compressed matter; therefore a cone tip is not required for preventing a hot plasma flowing into the cone [28]. The direct interaction of a dense matter with heating laser pulse is then realized with the open-tip cone, resulting in an enhancement of diffusive heating from the interaction zone to the imploded dense plasma.

Two-dimensional density profiles of compressed Cu(II) oleate solid balls were measured with a flash x-ray backlight technique coupled with a spherically bent crystal x-ray imager [29,30], as shown in Fig. 1. The magnification, spatial resolution, and spectral bandwidth were 20, 13 μm (FWHM), and 5 eV (FWHM), respectively. Details of this analysis are described in Ref. [14]. The converging shock waves were still traveling to the center of the solid ball at $t_{\mathrm{exp}} = 0.38$ ns; therefore the area close to the cone maintained the initial density of 1.1 g/cm^3. A maximum compression was reached at around $t_{\mathrm{exp}} = 0.72$ ns. The average mass density of the core along the laser axis is 11.3 g/cm^3.

Since the plasma compression progresses with time, we can experimentally test how isochoric heating efficiently changes with density, simply by altering the heating laser timing (e.g., $t_{\mathrm{exp}} = 0.37$ or 0.72 ns). Four LFEX beams

TABLE I. Summary.

Case	Shot ID	Heating energy (J)	Heating timing (ns)	Coupling (%)	Electron temperature (keV)	Mass density (g/cm^3)	Pressure (PPa)
A	40 558	1516	0.40	3.1 ± 0.5	2.1 ± 0.2	$1.1(+6.1/-0.0)$	$0.2(+1.4/-0.0)$
B	40 556	1016	0.61	4.3 ± 0.7	2.0 ± 0.1	$11.3(+5.9/-2.2)$	$2.2(+1.3/-0.5)$
C	40 547	1100	0.38	5.5 ± 0.9	1.9 ± 0.2	$1.1(+6.1/-0.0)$	$0.2(+1.4/-0.0)$
D	40 549	668	0.37	5.8 ± 0.9	1.5 ± 0.1	$1.1(+6.1/-0.0)$	$0.2(+1.4/-0.0)$
E	40 543	625	0.72	7.7 ± 1.2	NA[a]	$11.3(+5.9/-2.2)$	NA

[a]NA = not applicable.

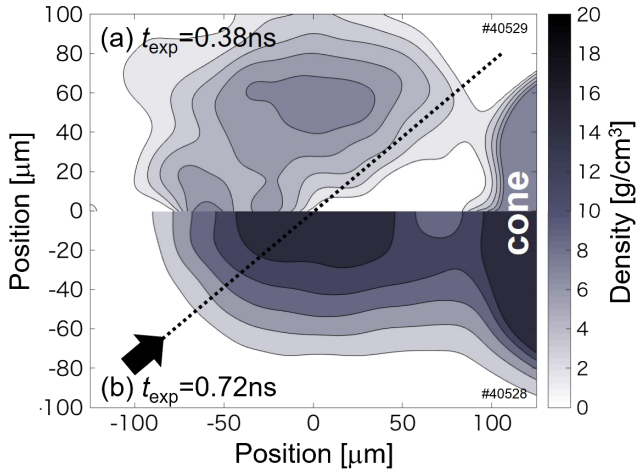

FIG. 1. Two-dimensional density profiles of compressed Cu (II) oleate solid balls. (a) At $t_{exp} = 0.38$ ns, the converging shock waves were still traveling to the center. (b) The core reached a maximum compression timing at $t_{exp} = 0.72$ ns. Dotted lines show line of sight of the x-ray spectrometer.

were injected from the gold cone to heat the compressed plasma isochorically to 1–2 keV. The wavelength, pulse shape, pulse duration, and energy of the LFEX beams were 1.053 μm, Gaussian, 1.8 ± 0.3 ps (FWHM), and varied from 620 to 1520 J. The focal spot diameter was 50 μm (FWHM) containing 30% of the total energy, yielding an intensity of 1.3×10^{19} W/cm^2 at the maximum energy shot. A short pulse laser system emits inevitably weak pulses preceding the main pulse. The intensity ratio of the main pulse to the preceding pulses is called the pulse contrast. A low contrast laser system produces a long-scale-length plasma in the laser-plasma interaction zone before the main pulse arrival time. The preformed plasma negatively affects the dense plasma heating because of the separation of the interaction zone away from the dense plasma. The high contrast LFEX laser enables an easy access to high density plasma.

The x-ray spectrometer was installed at 40° from the LFEX incident axis (dotted lines of Fig. 1). The spectrometer utilizes a planar highly oriented pyrolytic graphite as a dispersive element. The spectral resolution of the spectrometer was 17.9 eV (FWHM). Figures 2(a)–2(e) show x-ray spectra in the range of 8.0 to 8.6 keV. The peaks at 8.05, 8.35, and 8.39 keV are Cu-K_α, Li-like Cu satellite lines, and Cu-He_α, respectively. The peak at 8.26 keV is Ni-K_β that was emitted from a Ni-made capacitor-coil target. The peak around 8.5 keV is Au-L lines emitted from the Au cone. The ratio of Cu-He_α to the Li-like satellite line reflects information on the electron temperature T_e, plasma density ρ, and thickness along the line of sight of the spectrometer d.

X-ray spectra from Cu were computed by using the FLYCHK code [31]. The Ni-K_β and Au-L lines were measured in separate shots, and these emissions were subtracted from the measured spectra after adjusting their peak intensity to fit the measured one. The thickness was determined so that the spectrum could be reproduced within the density range obtained with the x-ray backlight. The spectra were calculated with varying ρ within the experimentally obtained density and T_e to minimize the differences between the experimental spectral shape and calculated ones.

In cases A, C, and D, where the LFEX is injected before the maximum compression timing, the minimum difference was found around 1.0 g/cm^3. The spectra calculated with $T_e = 2.1$, 1.9, and 1.5 keV, $\rho = 1.0$ g/cm^3, $d = 100$ μm well reproduce the shape of the spectrum, as shown in Figs. 2(a), 2(c), and 2(d), respectively.

The plasma was compressed further at the later timing (case B), the spectra calculated with $T_e = 2.0$ keV, $\rho = 12$ g/cm^3, $d = 30$ μm well reproduce the shape of the spectrum, see Fig. 2(b). In case B, our measurements show that the mass density of the plasma along the laser axis was 11.3 g/cm^3 and a part of the core was heated to 2.0 keV, which corresponds to 2.2 PPa of the electron

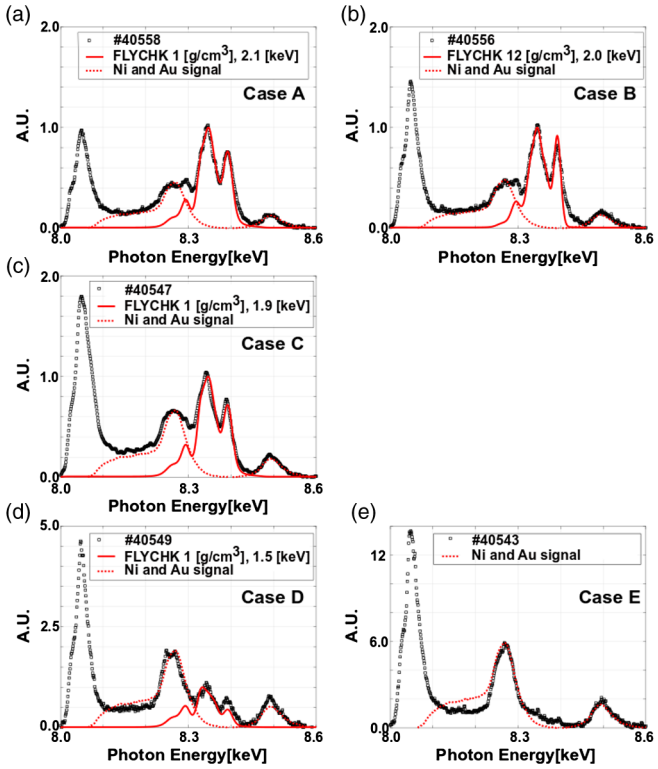

FIG. 2. X-ray spectra in the range from 8.0 to 8.6 keV. (a)–(e) Black square, red line, and red dotted line show the experimental spectra data, the computed spectra data by using the FLYCHK code, and the Ni-K_β and Au-L lines subtracted from the measured spectra. The experimental data of cases A, C, and D were well reproduced with the density 1.0 g/cm^3, and the temperature as 2.1 ± 0.2, 1.9 ± 0.2, 1.5 ± 0.1 keV, respectively. The experimental data of case B were well reproduced with the density 12 g/cm^3 and the temperature 2.0 ± 0.1 keV.

pressure. The amount of Li-like Cu satellite lines and Cu-He_α x-ray signal decreases as LFEX laser energy decreases. In case E, where the LFEX energy was at a minimum among the listed shots, the signal was too weak; therefore, it was impossible to evaluate the temperature by fitting as shown in Fig. 2(e). Details of the least square value of the differences between the measurements and calculations are presented in the Supplemental Material [15].

To identify the heated region, the heated core was imaged by the Fresnel phase zone plate (FPZP). He_α emissions indicating the heated region were observed along the laser axis, so that the experimental result confirms that the heating region exists in the above-solid-density region. Details of the FPZP observations are described in the Supplemental Material [15].

In our previous work, the maximum laser-to-core coupling efficiency by drag heating was $7.7\% \pm 1.2\%$, which corresponds to case E in Table I. It means that 48 ± 7 J energy can be deposited in the core by drag heating. Even at the maximum compression timing, the areal mass densities (ρL) of the core along the RE beam path length (L) were $\rho L = 0.16$ g/cm^2, which is shorter than the RE's mean free areal density (typically $\rho L = 0.6$ g/cm^2 for 1 MeV of the slope temperature of the RE). Therefore, the entire core was heated uniformly up to $T_e = 80 \pm 10$ eV by drag heating. Then, the $7.7\% \pm 1.2\%$ of coupling efficiency via the enhanced RE heating [14], which is so called drag heating, cannot explain the achievement of the UHED. This suggests that the other heating mechanism contributes predominantly to explain the observations.

We performed two-dimensional particle-in-cell (2D PIC) simulations (PICLS [32]) under an external magnetic field using the density distribution obtained in the experiment. The heating laser is similar to the LFEX laser. The detail of the simulations is given in the Supplemental Material [15].

Figure 3(a) shows the time evolution of the heated region indicated with contour lines of 1 keV from the heating laser peak time ($t = 0$) for the cases with the density profile at the maximum compression timing ($t_{\rm exp} = 0.72$ ns) in Fig. 1. The heating laser is irradiated from the right side through the cone and it heats directly the front edge of the dense plasma core owing to the high contrast laser light. The electron temperature evolves temporally via the thermal heat transport to the core by diffusive heating. The heat wave propagates with velocity > 10 μm/ps even after the heating laser irradiation terminated, and then the core region ($X < 40$ μm) was heated over 1 keV electron temperature at $t = 4.8$ ps, see Figs. 3(a) and 3(c). A theoretical estimation for the heat propagation speed is presented in the Supplemental Material [15].

Figure 3(b) shows the two-dimensional pressure distribution at $t = 4.8$ ps. The pressure of the core region ($X < 40$ μm) starts from 2 PPa at the front edge to 0.5 PPa at the other side ($X \simeq -10$ μm). Figure 3(c) shows the bulk electron temperature on the density distribution of

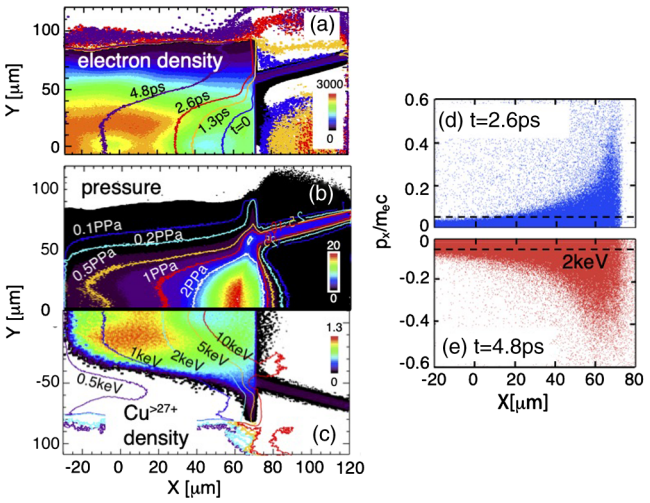

FIG. 3. PIC simulation at the maximum compression ($t_{\rm exp} = 0.72$ ns): (a) The propagation of heat wave indicated by 1 keV contour lines on the electron density [n_c]. (b) Pressure distributions with the contour lines (petapascal). (c) Electron temperature distribution on the doped copper density [n_c] with charge state $Z \geq 27$, which indicates where the He_α emissions come from. The contours are plotted at $t = 4.8$ ps after the heating laser peak time. The electron phase $X - p_x/m_e c$ at 2.6 ps (d) and 4.8 ps (e), lower half. The phase plot is vertically symmetric, so that only the upper and lower halves are shown due to the space limitation.

the doped copper having the charge states $Z \geq 27$. The doped copper densities with $Z \geq 27$ indicate that where Cu-He_α photons are coming from. We see that the doped copper ions inside the core region get $Z \geq 27$, namely, the large amount of He_α emissions are expected from the core. The core region at the maximum compression is heated to 1–2 keV, which is consistent with the experimental observation. The electron phase plots of the longitudinal momentum are shown in Figs. 3(d) and 3(e). The diffusive feature is seen from the heating surface ($X \sim 70$ μm). Note here that the phase plot is symmetric vertically in p_x space and also the phase plot of transverse momentum (p_y) has the identical distribution, namely, the electrons are thermalized in the momentum space in this energy range, < 10 keV. This PIC simulation reveals that diffusive heating is the heating process which can locally heat up the front region to the core region over petapascal pressure.

In summary, we have achieved experimentally 2.2 PPa of UHED state with 4.6 kJ of the total laser energy that is one order of magnitude lower than the energy used in the conventional implosion scheme. The generation of such the UHED state cannot be explained with drag heating mechanism only. Particle-in-cell simulations with the experimental conditions confirm that diffusive heating mechanism plays an essential role [4] to heat the core plasma over the kilo-electron-volt range on top of drag heating and resistive heating. Our experimental results clarified that the magnetized fast isochoric heating is an efficient way to create

the petapascal UHED state that is an interesting and unique test bed for various areas of scientific research, e.g., inertial confinement fusion, intense x ray, charged particles, neutron sources, and laboratory astrophysics. We must note that the ultrahigh pressure is realized in electron pressure, not in ion pressure. For fusion applications, we need ultrahigh ion pressure, and thus, further investigation is needed to shorten $T_e - T_i$ equilibration time to deliver ultrahigh ion pressure.

The authors thank the technical support staff of ILE and the Cyber Media Center at Osaka University for assistance with the laser operation, target fabrication, plasma diagnostics, and computer simulations. The authors thank Professor Santos and Dr. Bailly-Grandvaux (CELIA, University of Bordeaux) for fruitful discussion. This research used computational resources of the HPCI system provided by (Information Technology Center, Nagoya University) through the HPCI System Research Project (Project No. hp180093). This work was supported by the Collaboration Research Program between the National Institute for Fusion Science and the Institute of Laser Engineering at Osaka University (NIFS12KUGK057, NIFS15KUGK087, NIFS17KUGK111, and NIFS18KUGK118), and by the Japanese Ministry of Education, Science, Sports, and Culture through Grants-in-Aid, KAKENHI (Grants No. 24684044, No. 25630419, No. 15K17798, No. 15K21767, No. 15KK0163, No. 16K13918, No. 16H02245, and No. 17K05728), Bilateral Program for Supporting International Joint Research by JSPS, Grants-in-Aid for Fellows by Japan Society for The Promotion of Science (Grants No. 14J06592, No. 15J00850, No. 15J00902, No. 15J02622, No. 17J07212, No. 18J01627, No. 18J11119, and No. 18J11354), and the Matsuo Research Foundation.

[1] B. A. Remington, R. P. Drake, and D. D. Ryutov, Rev. Mod. Phys. **78**, 755 (2006).
[2] S. Fujioka *et al.*, Nat. Phys. **5**, 821 (2009).
[3] D. T. Casey *et al.*, Nat. Phys. **13**, 1227 (2017).
[4] H. Sawada *et al.*, Phys. Rev. Lett. **122**, 155002 (2019).
[5] S. M. Vinko *et al.*, Nat. Commun. **6**, 6397 (2015).
[6] R. Royle, Y. Sentoku, R. C. Mancini, I. Paraschiv, and T. Johzaki, Phys. Rev. E **95**, 063203 (2017).
[7] S. Le Pape *et al.*, Phys. Rev. Lett. **120**, 245003 (2018).
[8] S. P. Regan *et al.*, Phys. Rev. Lett. **117**, 025001 (2016).
[9] M. Tabak, J. Hammer, M. E. Glinsky, W. L. Kruer, S. C. Wilks, J. Woodworth, E. M. Campbell, M. D. Perry, and R. J. Mason, Phys. Plasmas **1**, 1626 (1994).
[10] R. Kodama, Nature (London) **412**, 798 (2001).
[11] W. Theobald *et al.*, Nat. Commun. **5**, 5785 (2014).
[12] L. C. Jarrott *et al.*, Nat. Phys. **12**, 499 (2016).
[13] A. J. Kemp, Y. Sentoku, V. Sotnikov, and S. C. Wilks, Phys. Rev. Lett. **97**, 235001 (2006).
[14] S. Sakata *et al.*, Nat. Commun. **9**, 3937 (2018).
[15] See Supplemental Material at http://link.aps.org/supplemental/10.1103/PhysRevLett.124.035001 for (1) schematics of the experimental layout; (2) mean square values of differences between measurements and calculations of the spectral analysis in the assumed density and temperature space; (3) description the quasimonochromatic imaging with a Fresnel phase zone plate to identify the heated region; (4) configurations of particle-in-cell (PIC) simulations; and (5) the model of diffusive heating for ignition design; which includes Refs. [16–20].
[16] Y. N. Denisiuk, Opt. Spectrosc. (USSR) **15**, 522 (1963).
[17] J. Kirz, J. Opt. Soc. Am. **64**, 301 (1974).
[18] A. Do, M. Briat, S. D. Baton, M. Krumrey, L. Lecherbourg, B. Loupias, F. Pérez, P. Renaudin, C. Rubbelynck, and Ph. Troussel, Rev. Sci. Instrum. **89**, 113702 (2018).
[19] Y. Iwasa, K. Yamanoi, Y. Kaneyasu, and T. Norimatsu, Fusion Sci. Technol. **73**, 258 (2018).
[20] T. Asahina, H. Nagatomo, A. Sunahara, T. Johzaki, and M. Hata, High Energy Density Phys. **30**, 8 (2019).
[21] K. F. F. Law *et al.*, Appl. Phys. Lett. **108**, 091104 (2016).
[22] S. Fujioka *et al.*, Sci. Rep. **3**, 1170 (2013).
[23] B. J. Zhu *et al.*, Appl. Phys. Lett. **107**, 241902 (2015).
[24] J. J. Santos *et al.*, New J. Phys. **17**, 083051 (2015).
[25] L. Gao *et al.*, Phys. Plasmas **23**, 043106 (2016).
[26] M. Bailly-Grandvaux *et al.*, Nat. Commun. **9**, 102 (2018).
[27] Y. Iwasa *et al.*, Fusion Eng. Des. **125**, 89 (2017).
[28] S. Fujioka *et al.*, Phys. Rev. E **91**, 063102 (2015).
[29] S. Fujioka, T. Fujiwara, M. Tanabe, H. Nishimura, H. Nagatomo, S. Ohira, Y. Inubushi, H. Shiraga, and H. Azechi, Rev. Sci. Instrum. **81**, 10E529 (2010).
[30] H. Sawada *et al.*, Appl. Phys. Lett. **108**, 254101 (2016).
[31] H. K. Chung, M. H. Chen, W. L. Morgan, Y. Ralchenko, and R. W. Lee, High Energy Density Phys. **1**, 3 (2005).
[32] Y. Sentoku and A. J. Kemp, J. Comput. Phys. **227**, 6846 (2008).